



# Interactive exploration of a 3D intracranial aneurysm wall model extracted from histologic slices

Annika Niemann<sup>1</sup> · Simon Weigand<sup>2</sup> · Thomas Hoffmann<sup>3</sup> · Martin Skalej<sup>4</sup> · Riikka Tulamo<sup>5</sup> · Bernhard Preim<sup>1</sup> · Sylvia Saalfeld<sup>1,3</sup>

Received: 30 July 2019 / Accepted: 18 October 2019 / Published online: 8 November 2019  
© CARS 2019

## Abstract

**Purpose** Currently no detailed in vivo imaging of the intracranial vessel wall exists. Ex vivo histologic images can provide information about the intracranial aneurysm (IA) wall composition that is useful for the understanding of IA development and rupture risk. For a 3D analysis, the 2D histologic slices must be incorporated in a 3D model which can be used for a spatial evaluation of the IA's morphology, including analysis of the IA neck.

**Methods** In 2D images of histologic slices, different wall layers were manually segmented and a 3D model was generated. The nuclei were automatically detected and classified as round or elongated, and a neural network-based wall type classification was performed. The information was combined in a software prototype visualization providing a unique view of the wall characteristics of an IA and allowing interactive exploration. Furthermore, the heterogeneity (as variance of the wall thickness) of the wall was evaluated.

**Result** A 3D model correctly representing the histologic data was reconstructed. The visualization integrating wall information was perceived as useful by a medical expert. The classification produces a plausible result.

**Conclusion** The usage of histologic images allows to create a 3D model with new information about the aneurysm wall. The model provides information about the wall thickness, its heterogeneity and, when performed on cadaveric samples, includes information about the transition between IA neck and sac.

**Keywords** Intracranial aneurysms · Aneurysm wall · Histologic images

---

✉ Annika Niemann  
annika.niemann@ovgu.de

Simon Weigand  
Simon.Weigand@med.uni-muenchen.de

Thomas Hoffmann  
t.hoffmann@ovgu.de

Martin Skalej  
martin.skalej@med.ovgu.de

Riikka Tulamo  
riikka.tulamo@helsinki.fi

Bernhard Preim  
bernhard.preim@ovgu.de

Sylvia Saalfeld  
sylvia.saalfeld@ovgu.de

<sup>1</sup> Faculty of Computer Science, Otto-von-Guericke University Magdeburg, Universitätsplatz 2, 39106 Magdeburg, Germany

<sup>2</sup> Ludwig-Maximilians-Universität Klinikum, Munich, Germany

## Introduction

The development of intracranial aneurysms (IAs) and the processes which lead to aneurysm rupture are still partially unknown. Different clinical parameters were found to influence the rupture risk, e.g. IA shape, size, location and patient age [1,2]. In this work, a 3D model of an IA from the anterior cerebral artery is generated based on histologic images to investigate the IA at the cellular level. Usually, 3D models of IAs are extracted from digital subtraction angiography (DSA) which is considered as a gold standard for IAs [3]. In clinical research, these models are employed for shape analysis and approximation of haemodynamics for rupture risk prediction [4].

<sup>3</sup> Research Campus STIMULATE, Magdeburg, Germany

<sup>4</sup> University Hospital Magdeburg, Magdeburg, Germany

<sup>5</sup> Helsinki University Hospital, University of Helsinki, Helsinki, Finland

Several studies exist on the development and remodelling of the IA wall and its role in aneurysm rupture. Costalat et al. [5] observed that wall tissue from unruptured IAs was more rigid than the tissue of ruptured ones based on material removed during surgical clipping. They did not find a correlation between wall thickness and rupture risk. Likewise Kataoka et al. [6] stated that the wall structures of ruptured and unruptured aneurysms differ. They found endothelial damage and an inflammatory cell invasion in ruptured IAs and introduced a wall structure score which was correlated with the score for inflammatory cell invasion. Frösen et al. [7] analysed IA tissue resected during surgery and found it was nearly intact at the neck and showed increasing degrees of degeneration (decrease in number of mural cells, mainly smooth muscle cells and wall thinning) in the direction of the dome. Frösen et al. [7] identified different wall types (endothelialized wall with linearly organized smooth muscle cells (SMC), thickened wall with disorganized SMC, hypocellular wall with either intimal hyperplasia or organizing luminal thrombosis and an extremely thin thrombosis-lined hypocellular wall) occurring in IAs. These wall types reflect changes in the aneurysm wall preceding aneurysm rupture. Histologic images show that complement system activation is correlated with aneurysm rupture [8]. Marbacher et al. [9] studied saccular, surgically created abdominal aortic aneurysms in rats and concluded that decellularization of the aneurysm wall increased neutrophil accumulation, wall inflammation and wall fragility and was associated with aneurysm growth.

While the reconstruction of a 3D model from histologic images is a new approach in IA research, histologic images were used for 3D models in other fields. Chakravarty et al. [10] used a manually segmented histologic data set, applied affine registration to the slices and created a brain atlas of the basal ganglia and the thalamus. Krauth et al. [11] used global affine registration and a B-spline controlled elastic deformation for the extraction of a brain atlas of the thalamic structures based on histologic data from several brains. A reference volume was created from one stack of histologic images and smoothed using surface nets. Can et al. [12] used a rigid registration for manually segmented histologic images of rhesus macaque monkeys' brains. They compared 3D histologic section images and MR images.

Upon wall identification itself, the analysis of cell nuclei can provide additional information about pathologic wall regions. The detection of nuclei in histologic images can be solved in different ways. Glaßer et al. [13] separated the nuclei from the background using Otsu's method. Additionally, they calculated the elongation, thickness and area of the nuclei and applied an agglomerative hierarchical clustering. Hafiane et al. [14] used fuzzy *c*-means with spatial constraints and active contours to detect nuclei in histologic images of

colon cancer. Chen et al. [15] as well as Sirinukunwattana et al. [16] solved nuclei detection problems with deep learning.

We provide a 3D model and interactive analysis tool of the 3D IA wall and include nuclei representation.

## Materials and methods

### Post-mortem intracranial aneurysm

The data set used in this work is an IA from a human cadaver with a ruptured aneurysm at the anterior cerebral artery. It was acquired in cooperation with the Forensic institute of the university hospital Magdeburg with approval of the local ethics committee. After embedding the aneurysm in paraffin, it was sliced axially to the aneurysm sac into 2- $\mu\text{m}$ -thick slices with a microtome. The slices were 100  $\mu\text{m}$  apart. They were haematoxylin and eosin (H&E) stained. As the slices are very thin, the problem of overlapping nuclei within one slice is avoided which simplifies the nuclei detection. Two consecutive slices were placed on a slide. The slides were scanned using a Hamamatsu Nanozoomer (Hamamatsu Photonics, Hamamatsu, Japan). The images had a resolution of 0.92  $\mu\text{m}$  per pixel and approx. 11,000  $\times$  8000 pixels. See also [13,17] for more information about the imaging.

### Model generation

The steps of our pipeline are illustrated in Fig. 1 and explained in the following.

**Preprocessing** The first step was to convert the ndpi files obtained by the scanner to tiff files using a tool from Deroulers et al. [18]. One file contains two slices. To get one file per slice, the images are cut parallel to the *y* axis. To cut the images, the samples are detected using Otsu's method [19] and an offset is added to the *x* expansion of the detected object before cutting the image. Images, where the automatic detection and cutting were problematic due to impurities, were manually processed.

**Segmentation** The vessel wall of larger arteries consists of three layers: adventitia, media and intima. The layers are separated by the external elastic membrane (between adventitia and media) and the internal elastic membrane (between media and intima) (see Fig. 2). Each layer consists of different cell types. Endothelial cells are found in the intima, smooth muscle cells in the media and stromal cells in the adventitia. During aneurysm development, the aneurysm wall changes and the layers become less distinguishable. However, often the histology still allows the identification of the inner, medial and outer (adventitial) parts of the wall.

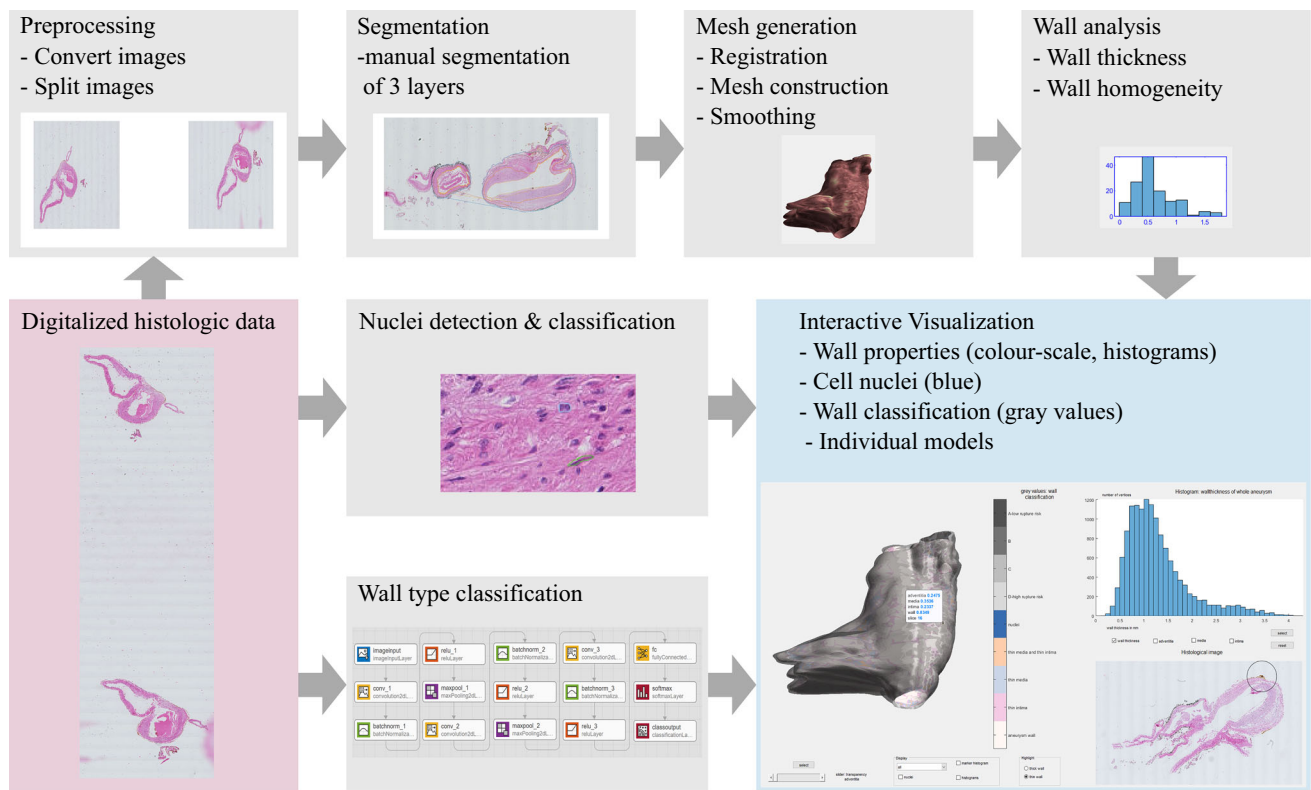


**Fig. 1** Pipeline of the proposed method to construct a 3D IA model from 2D histology

A manual segmentation by a medical expert was done using MeVisLab 2.8.1 (MeVis Medical Solutions AG, Bremen, Germany) [20]. The contours were exported as xml files. In MATLAB 2018b (MathWorks, Natick, USA), the contours were loaded and adjusted to match the coordinate system of the images. As shown in Fig. 2, the three layers of the IA are described by four contours: the inner contour (C1), the border between intimal and medial parts (C2), the border between medial and adventitial parts (C3) and the outer contour (C4).

**Mesh generation** Working with just the contours for the postprocessing instead of the histologic images significantly reduces the calculation time. The contours are resampled to have an equal number of points. The registration is limited to linear transformation without scaling to avoid invalid alternations of the contour or the wall thickness. To account for subsequent slices comprising the IA or a combination of the IA and its parent vessel, the contours' length was evaluated. In case of a significant difference in the length of two consecutive contours, the focus in registration was set on the aneurysm part (the part of the right side of the image, respectively, contour).

Since we obtained parallel contours with an equal number of points and a much better in plane resolution than the distance between the slices, approaches like Poisson surface

reconstruction did not yield satisfying results. Therefore, we directly triangulate the contours by connecting neighbouring points with their corresponding points of the next contour. Hence, the corresponding point of an arbitrary point of the first contour is defined as closest point on the subsequent contour. The corresponding points (points with corresponding indices) of two consecutive contours are connected. The contours can be sorted in a clockwise or a counterclockwise direction. After calculating the triangulation between two contours, one contour might be flipped, if that minimizes the length of the sum of all triangle edges.

This process is repeated for all four contours (C1–C4), resulting in four meshes (M1–M4) describing the three layers of the aneurysm. The mesh is smoothed with a manually Laplacian smoothing using Sculptis (Pixologic Sculptis).

## Wall analysis

From the four meshes, the thickness of the whole aneurysm wall as well as the thickness of each wall part is calculated. The wall thickness of the aneurysm wall is calculated for each vertex of the outer aneurysm mesh (M4) and approximated as the distance between the point on M4 and the closest point of the inner mesh (M1). The thickness of the wall layers is calculated similar: thickness of the intima as distance between M1 and M2, thickness of the media as

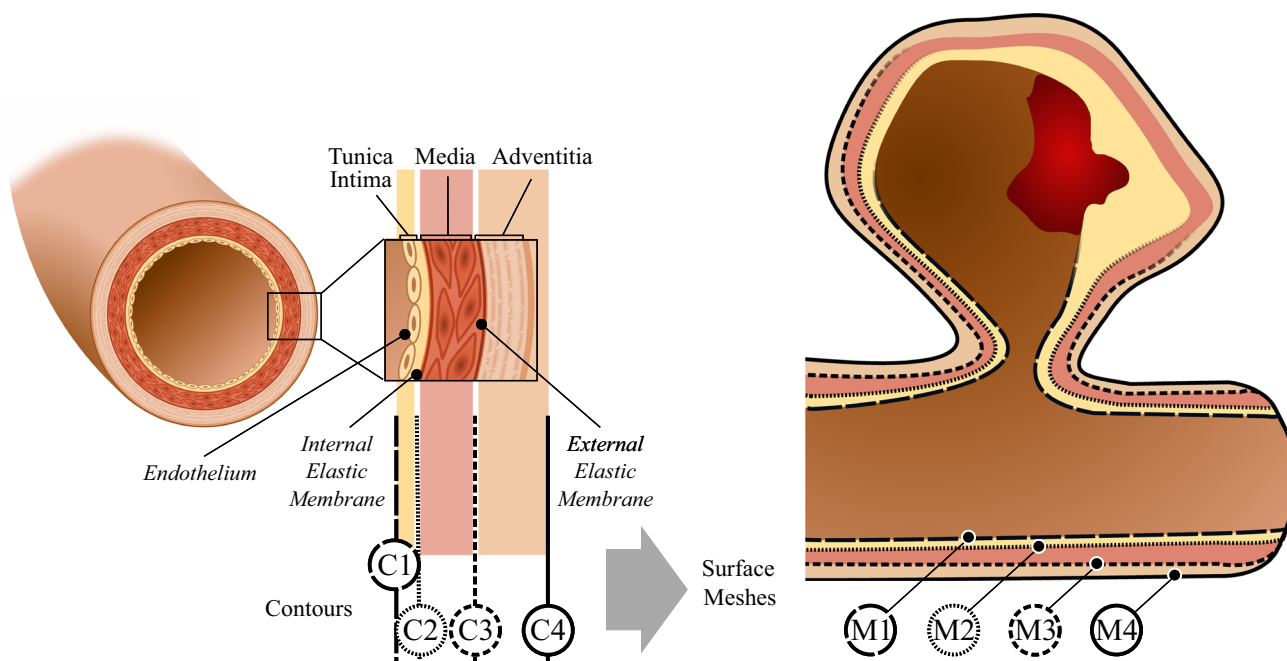


**Fig. 2** Schematic illustration of the extracted contours (C1–C4) of a normal artery and corresponding surface meshes (M1–M4) of an IA. The segmentation of the layers might be problematic in some IAs due to changes in the vessel wall occurring during aneurysm development.

Yellow area: myointimal hyperplasia/organized thrombus, dark red area inside IA: possible fresh thrombus (the IA used in this work did not have a fresh thrombus)

distance between M2 and M3 and the thickness of the adventitia as distance between M3 and M4. Due to changes in the aneurysm wall at some parts, the layers could only be approximated by using the neighbored slices. This might lead to slightly less precise calculations of the wall thickness of single layers compared to the calculation of the thickness of the whole aneurysm wall. Additional areas, where the overall wall thickness largely varies, are determined. For each vertex, its local neighbourhood is analysed and the standard variation of the corresponding wall thickness values is extracted. The size of the neighbourhood is determined such that 1% of the total vertex amount is considered.

**Nuclei detection** In the histologic images, the nuclei are detected and classified as round or elongated using the hierarchical clustering algorithm from Glaßer et al. [13].

**Wall classification** Our wall classification is adapted from Frösen et al. [7]. Based on 66 IAs (24 unruptured and 42 ruptured), they defined four tissue groups in IAs which are associated with different rupture tendencies. Type A has linearly organized smooth muscle cells, type B has a thickened wall with disorganized, proliferating smooth muscle cells, type C consists of a thick wall, decellularized of former myointimal hyperplasia or an organized thrombus and type D is extremely thin and decellularized with an organized

luminal thrombus [7]. A feed-forward neural net was trained using MATLAB and used to classify patches of the histologic images into four groups. The neural net consists of 15 layers, including several convolution, batch normalization, ReLU and pooling layers (see Fig. 3). The initial learn rate is 0.01 and is adapted using Adam [21]. The network was able to classify the patches of the aneurysm wall into four classes with an accuracy of 51.22%.

## Visualization

**Requirements** The main interest in aneurysm analyses is the risk of aneurysm rupture. Therefore, the visualization should show information about the aneurysm and its wall which are suspected to be related to rupture, like suspicious deformations, blebs, wall thickness and fine wall structure. Furthermore, information about the nuclei and the wall type classification should be incorporated in the visualization.

**Graphical user interface** The interface is split into two parts: on the left side, the 3D model is displayed, and on the right side, a histogram and the histologic image are shown (see Fig. 5). In the 3D overview, the mesh M3 is colour-coded to highlight either the thin parts of media and intima or the thick parts of media and intima, depending on the user selection. The thickness of the adventitia is shown by adding

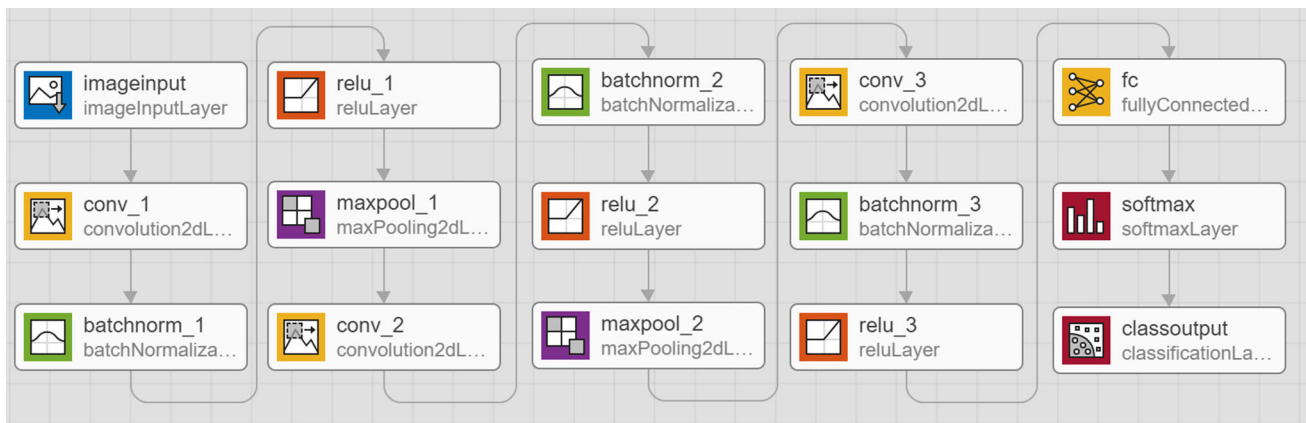


**Fig. 3** Architecture of the neural net used to classify the aneurysm wall, visualized with MATLAB [MathWorks, MATLAB (2018b)]. 1 ‘imageinput’—image input  $500 \times 500 \times 1$  images with zero centre normalization. 2 ‘conv\_1’ Convolution— $8 \times 3 \times 3 \times 1$  convolutions with stride [1 1] and padding ‘same’. 3 ‘batchnorm\_1’ Batch Normalization—batch normalization with 8 channels. 4 ‘relu\_1’ ReLU—ReLU. 5 ‘maxpool\_1’ Max Pooling— $2 \times 2$  max pooling with stride [2 2] and padding [0 0 0 0]. 6 ‘conv\_2’ Convolution— $16 \times 3 \times 3 \times 8$  convolutions with stride [1 1] and padding ‘same’. 7 ‘batchnorm\_2’

Batch Normalization—batch normalization with 16 channels. 8 ‘relu\_2’ ReLU—ReLU. 9 ‘maxpool\_2’ Max Pooling— $2 \times 2$  max pooling with stride [2 2] and padding [0 0 0 0]. 10 ‘conv\_3’ Convolution— $32 \times 3 \times 3 \times 16$  convolutions with stride [1 1] and padding ‘same’. 11 ‘batchnorm\_3’ Batch Normalization—batch normalization with 32 channels. 12 ‘relu\_3’ ReLU—ReLU. 13 ‘fc’ Fully Connected—5 fully connected layers. 14 ‘softmax’ Softmax—softmax. 15 ‘classoutput’—classification output

M4 as a semi-transparent layer around M3 (see Fig. 5). On M4, the wall type classification is transparently displayed with a grey colour map. Wall parts with a higher rupture tendency according to the classification have a lighter grey tone and a lower rupture tendency is displayed as a darker grey. The lighter grey allows a good perception of the underlying colour-coded surface, thus helping to focus on the wall at areas with a higher tendency to rupture. The user can choose additional information to be displayed in the 3D model. Glyphs displaying the round nuclei can be added; see Fig. 4. The glyphs are blue balls representing the number of nuclei in that area with their size. Heterogeneous wall parts, here defined as wall parts with a high variance in wall thickness, are shown using small histograms around the 3D model. One histogram shows the distribution of the wall thickness around the current point, and the other three show especially heterogeneous parts. For these histograms, the corresponding areas on the 3D model are displayed with markers on the surface. The marker colour and the colour of the histogram axis match.

Instead of the overview model, the user can select only one of the four surface models (M1–M4) and colour-coding of the wall thickness of the selected aneurysm layer is shown accordingly; see Fig. 6. The model allows the user to select one point from a model to examine the measurements, e.g. wall thickness, from that point only. Afterwards, the corresponding histologic image is loaded and displayed in the GUI; see bottom right of Fig. 5. A circle marks the corresponding area in the histologic image to the selected point. Due to the smoothing of the model, small variations are

induced, and therefore, the circular area rather than a precise location is shown.

We also provide a histogram-based wall thickness selection. On the upper right side, a histogram of the wall thickness is displayed. The user may select one or more histograms (histogram of whole aneurysm wall thickness, thickness of adventitia, thickness of media or thickness of intima) to be displayed. In the histogram, the user can interactively select one or more bars. Then, the corresponding areas with these wall thicknesses are highlighted in the 3D model; recall Fig. 4.

## Results

Since we do not have access to an additional imaging of the intracranial aneurysm or its wall, it was not possible to make a quantitative comparison with another model based on in vivo or ex vivo imaging. The generated 3D models and the resulting wall thickness were evaluated by using the user interface and the described point selection to compare the model with the corresponding image data. The model seems to correctly reproduce the aneurysm as shown in the histologic image data.

Due to the limited data, a quantitative evaluation of the wall classification would not be suitable. The result of the neural net is plausible, as the classification shows a lower rupture risk towards the parent vessel and a higher rupture risk in the direction of the aneurysm dome. Aneurysms normally rupture at the dome (83–84%) and only 2% at the neck [8]. Therefore, the results fit the expectations.

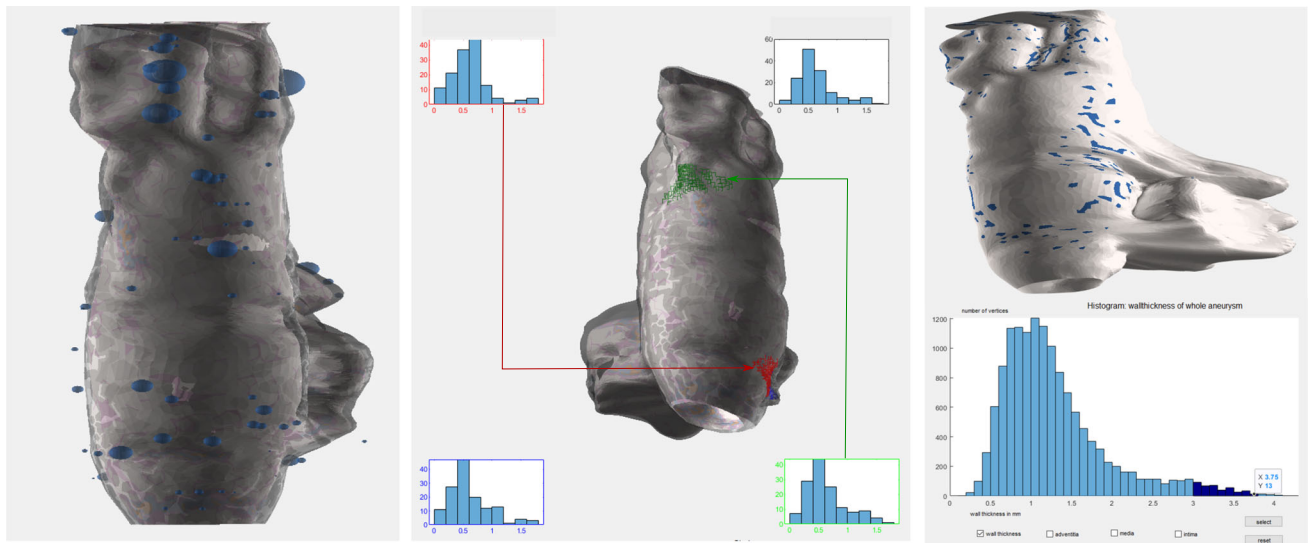


**Fig. 4** Interactive exploration of the wall of the intracranial aneurysm. Left: 3D model and nuclei at selected positions. Centre: Local histograms ( $x$  axis: wall thickness,  $y$  axis: number of vertices) showing the

distribution of the local wall thickness. Right: Histogram-based selection of wall thickness (bottom right) and corresponding highlighting of affected areas (top right)

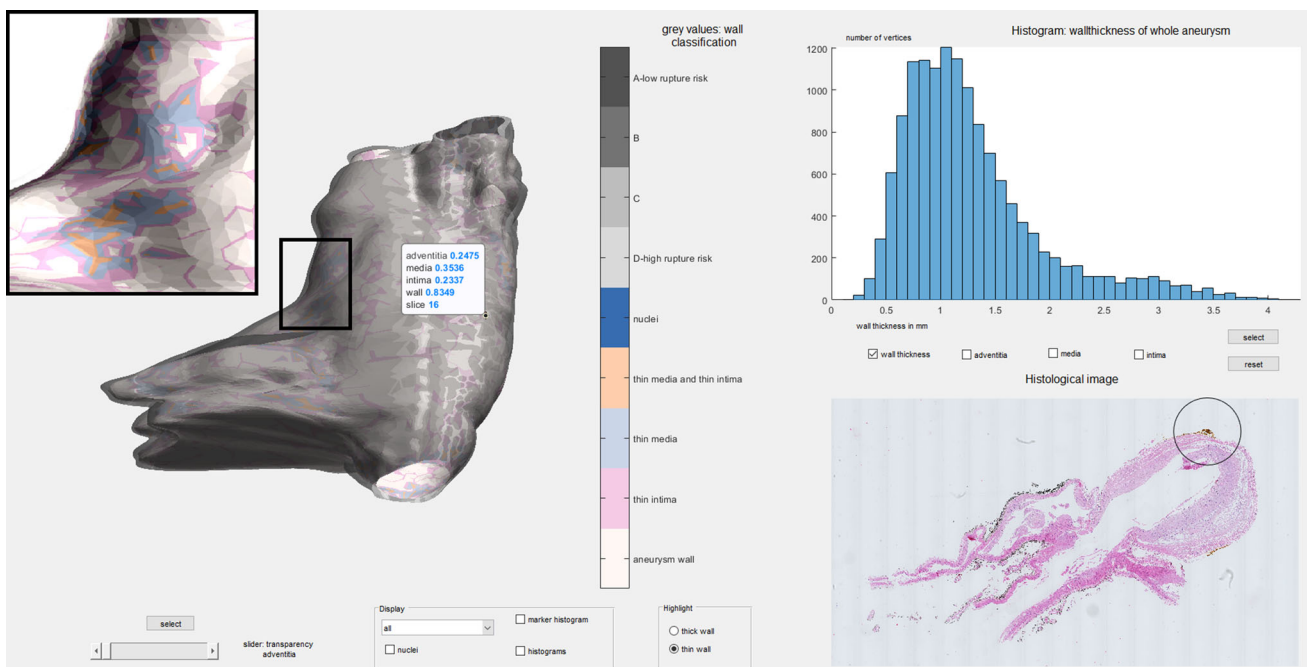


**Fig. 5** Graphical user interface to explore the wall thickness of a cerebral aneurysm: left: overview visualization showing wall thickness and wall classification, right: histogram of wall thickness and histologic

image; black rectangle: zoomed in view of surface; circle on histologic image: origin of selected point

## Discussion

We presented our tool to a medical expert yielding an overall positive feedback. She was interested in seeing a 3D model of the histologic data and particular liked the histogram-based selection of areas with a certain wall thickness. She com-

mented that, while being interesting, the areas analysed with regard to wall heterogeneity could be larger and she would like to see further analysis of the wall and the cells occurring inside.

Despite the small data set for the wall classification, the neural net produces a plausible result. Due to the small

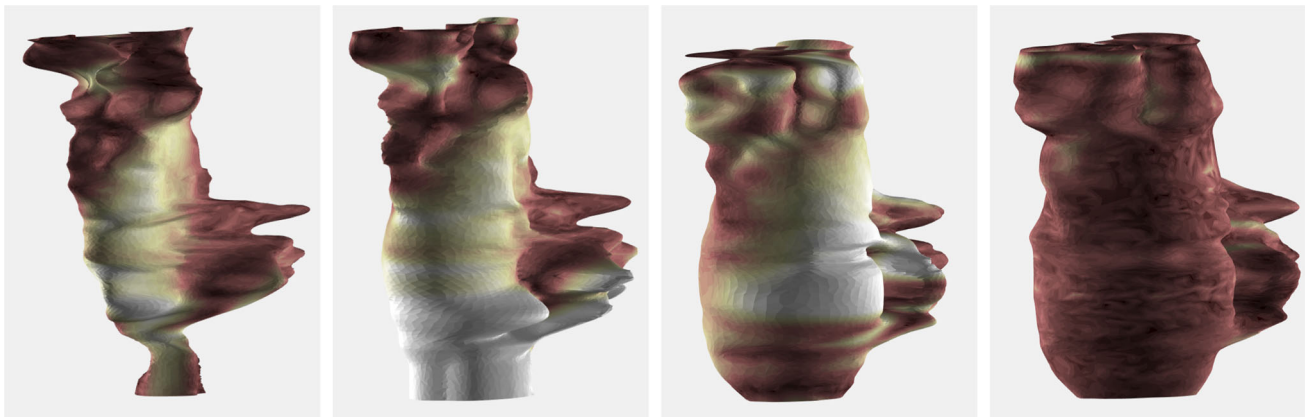


**Fig. 6** Models M1, M2, M3 and M4 (from left to right) representing the aneurysm wall. The white area in M3 is a particularly thick wall part. The colour scale is consistent over all four views for an easy comparison of different wall layers

amount of data, we cannot present statistical significant and meaningful results. When analysing first trends, then we can state that the aneurysm dome is correlated with a higher rupture risk than the neck or the parent vessel. This suggested that deep learning for IA wall classification might be a suitable approach if a sufficient number of examples are available. The results might be further improved by combining the classification of smaller patches to classify larger areas. While here every part of the presented model was classified, the classification has been created and is currently only researched for the aneurysm dome and not the aneurysm neck or the parent vessel. Additional research is necessary to analyse changes in the neck area and parent vessel.

The segmentation of different IA layers is arguable. Vessel wall changes occur during IA development yielding less distinguishable layers. In particular, IAs existing over a longer period undergo wall remodelling that may fade out the general artery wall layers and a more general approach based on inner and outer vessel walls might be required. Although we were able to approximate a distinction between these layers, this might not be possible for more advanced IAs. In the future, instead of these layers, a division of the aneurysm wall as described might be necessary [5,6,8,9].

The data set presented in this work is special as it includes both the aneurysm dome and the neck. Compared to the resection of aneurysm domes during surgical intervention, the collection of whole aneurysms from cadavers is more complex and rarely done. In particular, the analysis of the aneurysm neck and parent vessel can only be carried out *ex vivo*. However, the histologic images of this data set did not show a thrombus. As a thrombus might be found in an IA, future analysis and visualization should take this into account.

The analysis of the nuclei is more restricted than the analysis of whole cells. This work focused on round nuclei which provide limited information about the cellular composition

of the wall. Future wall analysis should be more comprehensive and use whole cells with cell-specific histologic markers instead of focusing on the nuclei in order to enable verification between different cell types.

In this model, the wall thickness and aneurysm shape are influenced by the generation of the image data. A slight deformation of the aneurysm could occur during the processing. Fixation and preparation of pathologic sections may further induce potential bias due to the loss of water during the processes. In the previous work, we observed a statistically significant bias for the *ex vivo* measurements of healthy intracranial vessel wall diameters when comparing histology and intravascular imaging [17]. However, there was a negligible shrinkage of fibrotic tissue and plaques, assumedly due to the already reduced water content of these pathologies. During the processing, small parts of the tissue at the inner and outer borders start to separate from the rest of the tissue. This complicates the correct segmentation of the aneurysm contour and could lead to small inaccuracies in the segmentation and the model. Thus, the current methodology leaves room for an error in measuring the wall thickness. However, currently this is one of the few methods enabling the measurement of the wall thickness of the IA samples *ex vivo*.

Currently the IA wall thickness cannot be evaluated reliably by CT or MR imaging *in vivo* due to relatively low resolution in comparison with the thin wall of an aneurysm. Besides histologic images, the usage of optical coherence tomography data for IA wall thickness visualization is promising [13]. Another alternative for *ex vivo* analysis of wall composition is multiphoton microscopy as employed by Robertson et al. [22]. They combined it with mechanical testing of the samples, including measurement of the wall thickness at five positions using micro-callipers. The study used IA domes resected during surgical clipping.

Part of the current IA research relies on simulations which aim at finding parameters associated with aneurysm

rupture [23]. In the future, the 3D model of an aneurysm described here could be used to simulate the blood flow including mechanical properties for fluid–structure interactions to provide further insight in aneurysm rupture and the influence of the patient-specific aneurysm wall thickness on the intra-aneurysmal blood flow. Finally, a 3D model incorporating the extracted histologic information could increase the understanding of the aneurysm pathology and thus help with IA diagnostics and treatment in the future.

## Conclusion

This work presents a virtual 3D model of an IA from the anterior cerebral artery and its different wall layers which is based on histologic image data. This is the first human 3D model of a complete IA from histologic image data. The model based on a cadaveric sample includes the patient-specific wall thickness and shows the aneurysm as well as the transition between the aneurysm sac and the parent vessel. Embedded in our visual exploration software tool, an interactive analysis of the aneurysm and its heterogeneity is available.

**Acknowledgements** This work is partly funded by the German Research Foundation (SA 3461/2-1) and the Federal Ministry of Education and Research within the Forschungscampus *STIMULATE* (13GW0095A).

## Compliance with ethical standards

**Conflict of interest** All authors declare that they have no conflict of interest.

**Ethical standards** All procedures performed in studies involving human participants were in accordance with the ethical standards of the institutional and/or national research committee and with the 1964 Helsinki Declaration and its later amendments or comparable ethical standards. For this type of study, formal consent is not required.

## References

- Juvela S, Porras M, Poussa K (2000) Natural history of unruptured intracranial aneurysms: probability of and risk factors for aneurysm rupture. *J Neurosurg* 93(3):379–387
- Raghavan LM, Baoshun S, Harbaugh R (2005) Quantified aneurysm shape and rupture risk. *J Neurosurg* 102(2):355–362
- Geers AJ, Larrabide I, Radaelli AG, Bogunovic H, Van Andel HAFG, Majoie CB, Frangi AF (2009) Reproducibility of image-based computational hemodynamics in intracranial aneurysms: comparison of CTA and 3DRA. In: *IEEE International symposium on biomedical imaging: From Nano to Macro*, pp 610–613
- Berg P, Voß S, Janiga G, Saalfeld S, Bergersen AW, Valen-Sendstad K, Bruening J, Goubergrits L, Spuler A, Chiu TL, Tsang ACO, Copelli G, Csippa B, Paál G, Závodszy G, Detmer FJ, Chung BJ, Cebra JR, Fujimura S, Takao H, Karmonik C, Elias S, Cancelliere NM, Najafi M, Steinman DA, Pereira VM, Piskin S, Finol EA, Pravdivtseva M, Velvaluri P, Rajabzadeh-Oghaz H, Paliwal N, Meng H, Seshadhri S, Venguru S, Shojima M, Sindeev S, Frolov S, Qian Y, Wu Y, Carlson KD, Kallmes DF, Dragomir-Daescu D, Beuing O (2019) Multiple Aneurysms AnaTomy CHallenge 2018 (MATCH)–phase II: rupture risk assessment. *Int J Comput Assist Radiol Surg* 14(10):1795–1804
- Costalat V, Sanchez M, Ambard D, Thines L, Lonjon N, Nicoud F, Brunel H, Lejeune JP, Dufour H, Bouillot P, Lhalcky JP, Kouri K, Segnarbieux F, Maurage CA, Lobotesis K, Villa-Uriol MC, Zhang C, Frangi A, Mercier G, Bonafé A, Sarry L, Jourdan F (2011) Biomechanical wall properties of human intracranial aneurysms resected following surgical clipping. *J Biomech* 44(15):2685–2691
- Kataoka K, Taneda M, Asai T, Kinoshita A, Ito M, Kuroda R (1999) Structural fragility and inflammatory response of ruptured cerebral aneurysms. A comparative study between ruptured and unruptured cerebral aneurysms. *Stroke* 30(7):1396–1401
- Frösen J, Piippo A, Paetau A, Kangasniemi M, Niemelä M, Hernesniemi J, Jääskeläinen J (2004) Remodeling of saccular cerebral artery aneurysm wall is associated with rupture: histological analysis of 24 unruptured and 42 ruptured cases. *Stroke* 35(10):2287–2293
- Tulamo R, Frösen J, Hernesniemi J, Niemela M (2010) Inflammatory changes in the aneurysm wall: a review. *J NeuroInterventional Surg* 2(2):120–130
- Marbacher S, Marjamaa J, Bradacova K, von Gunten M, Honkanen P, Abo-Ramadan U, Hernesniemi J, Niemelä M, Frösen J (2014) Loss of mural cells leads to wall degeneration, aneurysm growth, and eventual rupture in a rat aneurysm model. *Stroke* 45(1):248–254
- Chakravarty M, Bertrand G, Hodge CP, Sadikot AF, Collins DL (2006) The creation of a brain atlas for image guided neurosurgery using serial histological data. *NeuroImage* 30(2):359–376
- Krauth A, Blanc R, Poveda A, Jeanmonod D, Morel A, Székely G (2010) A mean three-dimensional atlas of the human thalamus: generation from multiple histological data. *NeuroImage* 49(3):2053–2062
- Can C, Lei W, Lynn S, John C, Michael M, Tilak RJ (2010) Large deformation diffeomorphic metric mapping registration of reconstructed 3D histological section images and in vivo MR images. *Front Hum Neurosci* 4(43):1–12
- Glaßer S, Hoffmann T, Boese A, Voß S, Kalinski T, Skalej M, Preim B (2017) Virtual inflation of the cerebral artery wall for the integrated exploration of OCT and histology data. *Comput Graph Forum* 36(8):57–68
- Hafiane A, Bunyak F, Palaniappan K (2008) Fuzzy clustering and active contours for histopathology image segmentation and nuclei detection. *Adv Concepts Intell Vis Syst* 5259:903–914
- Chen H, Qi X, Yu L, Dou Q, Qin J, Heng P (2017) DCAN: deep contour-aware networks for object instance segmentation from histology images. *Med Image Anal* 36:135–146
- Sirinukunwattana K, Raza S, Tsang Y, Snead DRJ, Cree IA, Rajpoot NM (2016) Locality sensitive deep learning for detection and classification of nuclei in routine colon cancer histology images. *IEEE Trans Med Imaging* 35(5):1196–1206
- Weigand S, Saalfeld S, Hoffmann T, Eppler E, Kalinski T, Jachau K, Skalej M (2019) Suitability of intravascular imaging for assessment of cerebrovascular diseases. *Neuroradiology*. <https://doi.org/10.1007/s00234-019-02233-w>
- Deroulers C, Ameisen D, Badoual M, Gerin C, Granier A, Lartaud M (2013) Analyzing huge pathology images with open source software. *Diagn Pathol* 8(1):92
- Otsu N (1979) A threshold selection method from gray-level histograms. *IEEE Trans Syst Man Cybern* 9(1):62–66
- Ritter F, Boskamp T, Homeyer A, Laue H, Schwier M, Link F, Peitgen H (2011) Medical image analysis. *IEEE Pulse* 2(6):60–70
- Diederik KP, Ba AJ (2015) A method for stochastic optimization. In: *3rd International conference for learning representations*, pp 1–13

22. Robertson AM, Duan X, Aziz KM, Hill MR, Watkins SC, Cebra JR (2015) Diversity in the strength and structure of unruptured cerebral aneurysms. *Ann Biomed Eng* 43(7):1502–1515
23. Voß S, Saalfeld S, Hoffmann T, Beuing O, Weigand S, Jachau K, Preim B, Thévenin D, Janiga G, Berg P (2016) Fluid-structure simulations of a ruptured intracranial aneurysm: constant versus patient-specific wall thickness. *Comput Math Methods Med* 1–8:2016

**Publisher's Note** Springer Nature remains neutral with regard to jurisdictional claims in published maps and institutional affiliations.